Available online at www.sciencedirect.com
ScienceDirect
Optics Communications 270 (2007) 255–261
OPTICS COMMUNICATIONS
www.elsevier.com/locate/optcom

Bose–Einstein condensation of metastable helium in a bi-planar quadrupole Ioffe configuration trap

R.G. Dall, A.G. Truscott *

ARC Centre of Excellence for Quantum-Atom Optics, Research School of Physical Sciences and Engineering, Australian National University, Canberra, ACT 0200, Australia

Received 25 May 2006; received in revised form 25 August 2006; accepted 9 September 2006

Abstract

Using a novel magnetic trapping geometry we have evaporatively cooled metastable helium atoms to form a Bose–Einstein condensate containing approximately one million atoms. This is only the fourth demonstration of a metastable condensate and the first realisation of a BEC in a bi-planar quadrupole Ioffe configuration magnetic trap.
© 2006 Elsevier B.V. All rights reserved.

Keywords: Metastable helium; Bose–Einstein condensation; Magnetic trapping

1. Introduction

The first realizations of Bose–Einstein condensation (BEC) in a dilute gas of weakly interacting atoms [1–3], have led to an explosion of research in the field of quantum degenerate gases. These first demonstrations were all achieved with alkali atoms in their true electronic ground state. In 2001, two groups [4,5] successfully created the worlds first metastable BEC, comprising metastable 2^3S_1 helium atoms (He^*). It had long been thought such an achievement would be impossible due to Penning ionisation: two colliding He^* atoms have a combined internal energy of ~40 eV which is sufficient to ionize one of the collision partners while transferring the other to the ground state. However, as predicted by Shlyapnikov et al. [6], Penning losses are reduced by four orders of magnitude in a magnetic trap of He^*, compared to an unpolarised sample, and thus these losses did not stop the production of a He^* BEC.

The large internal energy of metastables makes them interesting candidates for BEC, allowing single atom detection with high spatial (μm) and temporal resolution (ns). Recently, Schellekens et al. made use of this unique property to demonstrate the Hanbury–Brown Twiss effect with He^* atoms [7]. Another unique property of a He^* BEC is that it produces ions due to Penning ionisation. This process allows the experimenter a very sensitive tool, to non-destructively monitor the condensate in real time. Seidelin et al. were able to map out the evolution of a BEC, from formation to decay, using this unique tool [8].

Besides the unique detection possibilities that He^* offers, it is also attractive to the spectroscopist due to its relatively simple atomic structure. He^* has only two electrons and no hyperfine interaction, and thus its energy levels can be calculated with a high degree of accuracy. In 2003, Léonard et al. [9] used photoassociation to spectroscopically demonstrate the presence of long range molecular bound states of He^*. The experimentally determined binding energies were in excellent agreement with theoretical predictions. More recently, spectroscopic measurements of the s-wave scattering length of He^* have been achieved with unprecedented accuracy by Leduc and co-workers [10].

In this paper, we report on our realisation of a BEC of He^*. This represents only the fourth such achievement of a metastable BEC. Our experimental system is quite different

* Corresponding author. Tel.: +61 2 61253626.
E-mail address: andrew.truscott@anu.edu.au (A.G. Truscott).

0030-4018/$ - see front matter © 2006 Elsevier B.V. All rights reserved.
doi:10.1016/j.optcom.2006.09.031

from the three other successful He* BEC experiments [4,5,11], the major difference being our magnetic trapping geometry. Our magnetic trap is similiar to a quadrupole Ioffe configuration (QUIC) trap [12], except instead of the usual Ioffe coil, we use two coils in an anti-Helmholtz (AH) arrangement to produce the Ioffe field. The big advantage of this trapping geometry is that it requires only two spatial planes, rather than the three needed for the standard QUIC trap. This bi-planar quadrupole Ioffe configuration (BiQUIC) trap offers better optical access than the standard QUIC trap, but still produces strong confinement with minimal amp-turns. Until now, almost all BEC experiments, which use large metal vacuum chambers have used cloverleaf type magnetic traps [13], since the three spatial planes required for the standard QUIC trap have prohibited its use.

2. Experimental setup

In our experimental setup we use a cryogenically cooled DC discharge to produce our source of He*. The design and performance of this source have been reported elsewhere [14]. The source is cooled with either liquid nitrogen or liquid helium, the latter providing a slower and more intense He* beam [17]. The He* atomic beam is first collimated in a 2-dimensional optical molasses and then bent by 1.7° off axis, using a second collimation stage tilted at the required bending angle. After the bending stage a Zeeman slower [15] is used to slow the atoms down to ~70 m/s, at which point they can be captured by our first magneto-optic trap (MOT). Due to the low production efficiency of metastables, only about 1 in 10^4 helium atoms are excited into the metastable state [16], resulting in a large amount of background helium reaching the first MOT chamber. This is despite 3 stages of differential pumping and reduction of line-of-sight source He atoms which are not bent by our bending stage. The result is that the partial pressure of helium is $\sim 5 \times 10^{-9}$ torr in our first MOT, far too high to allow the production of a BEC. To circumvent this problem we transfer atoms from this chamber into a region of much higher vacuum, by implementing a similar scheme to that of the low velocity intense source (LVIS) first demonstrated by Lu et al. [18].

Our transfer method is an extension of the work of Lu et al. In their experiments a narrow dark column was placed in one of the MOT laser beams, and radiation pressure imbalances forced the atoms out of the MOT and into an atomic beam or LVIS. We use a retro-optic with a small ~1.5 mm hole in it to generate a dark column in one of our MOT beams. However we also use an additional *push* beam to produce our atomic beam or LVIS$^+$. The experimental details and performance of our LVIS$^+$ have been described in detail elsewhere [19]. However for the purposes of loading a second MOT in a region of higher vacuum the most important results are the maximum obtainable flux of 2×10^{10} atoms/s (as measured at the trapping region), the longitudinal velocity of the beam ~40 m/s and a beam divergence ⩽45 mRad.

2.1. Second magneto-optic trap

The use of an LVIS$^+$ atomic beam to load our second MOT has many advantages. A schematic of our second MOT loading geometry is shown in Fig. 1. Firstly, the setup allows for differential pumping between the two MOT stages, reducing the partial pressure of residual helium by a factor of approximately 1000 in the BEC chamber. Secondly, the longitudinal velocity of the atomic beam is lower than that achievable from a He* Zeeman slowed beam by a factor of ~2. This is important, since the distance required for a MOT to slow and subsequently capture an atom scales as the square of the velocity. Thus our second MOT has laser beam diameters ~12 mm, rather than the ~38 mm diameter beams the first MOT requires. Finally, the small divergence of the LVIS$^+$ beam is critical to our experimental setup, since it allows us to produce a second MOT within a small trapping volume. As a result the re-entrant vacuum windows, which our BiQUIC magnetic trap locates against, can be separated by only 9 mm (see Fig. 1) with only minimal disruption of our second MOT. The small separation of our BiQUIC coils allows us to generate a tight confining magnetic trap with only a minimum amount of amp-turns required, this will be discussed further in the next section.

Our second MOT is comprised of four sets of retro-reflected laser beams, three in the usual MOT configuration [20], and an additional pair at a 15° angle from the horizontal. These extra beams increase the capture velocity of our MOT and improve our final atom number by approxi-

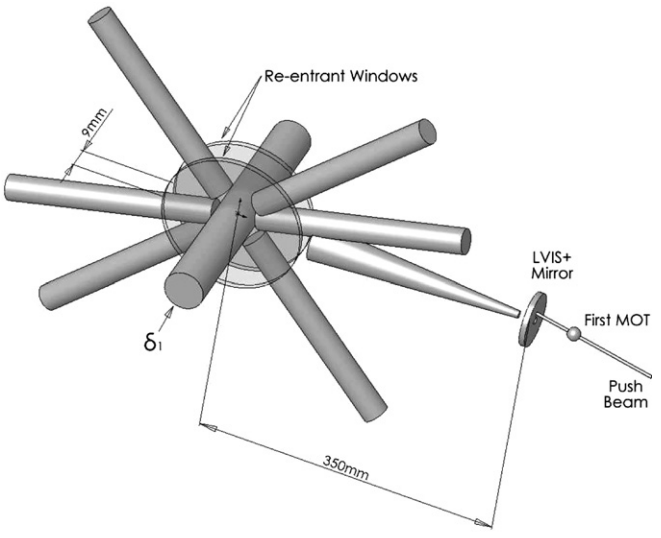

Fig. 1. Schematic of our second MOT loading scheme. The re-entrant windows that the BiQUIC coils locate against are shown along with our eight MOT laser beams. The horizontal MOT laser beam detuning is denoted δ_1 and is closer to resonance than the rest of the MOT beams, which are detuned by δ_2.

mately a factor of two. Our MOT also differs from a conventional MOT in that the horizontal laser beams, as shown in Fig. 1, have a smaller detuning than the other MOT beams. The reduced detuning stiffens the trap in the dimension which is restricted to 9 mm and thus reduces losses caused by atoms hitting our re-entrant windows. The use of two MOT detunings increases our atom number by a factor of two. The trapping field for the second MOT is provided by an independent set of 12 cm diameter AH coils. With the laser beam detunings for the second MOT set to $\delta_1 = -13\Gamma$ and $\delta_2 = -20\Gamma$ (where $\Gamma = 1.6$ MHz is the natural linewdith) and their respective intensities per beam set to $I_1 = 3I_{\text{sat}}$ and $I_2 = 37I_{\text{sat}}$ (where $I_{\text{sat}} = 0.17\ \text{mW/cm}^2$), and a trapping field gradient in the strong axis of 31 G/cm, we are able to routinely load 5×10^8 atoms into our MOT with a temperature of 1 mK.

2.2. Magnetic trap

In general there are three standard magnetic traps used in BEC experiments: the TOP trap [1], the cloverleaf trap [13] and the QUIC trap [12]. The TOP trap was the first trap in which BEC was successfully achieved, however its application is somewhat limited due to the low trap depth and technical difficulties associated with its rotating field. A cloverleaf magnetic trap, is generated with three sets of coils, a quadrupole set, a bias set and a curvature set. The quadrupole set, has a relatively complicated coil layout, with a single coil of the set resembling a '*cloverleaf*'. Despite its complexity the cloverleaf trap is routinely used in BEC experiments and offers some advantages over the QUIC trap. These are the ability to independently control the axial and radial trap frequencies and bias field, and the fact that the magnetic field zero lies in the centre of the coil set. The simplest magnetic trap is the QUIC trap, consisting of just three coils, one set in AH configuration and a third Ioffe coil in a plane orthogonal to the AH set. Despite its simplicity, a conventional QUIC trap has one major drawback: its geometry requires access to three planes. Moreover, these three planes need to be relatively close to one another. This requirement is difficult to meet in many experiments where a large vacuum chamber is needed, such as ours. Thus the standard QUIC trap is usually only applicable, to BEC experiments using small glass cells. This problem is alleviated with our BiQUIC geometry in which we replace the single Ioffe coil with a second AH set, such that the trap only requires two spatial planes.

Our BiQUIC geometry is shown in Fig. 2. It consists of two sets of AH coils, the first producing the quadrupole field for r confinement while the second set is used to allow a non-zero bias field and harmonic confinement in the z direction. In our setup the separation between each coil of a single AH set is ~17 mm, this small separation enables us to generate tight trapping frequencies with a minimum of amp-turns. For an AH set of coils the scaling between the separation of the coils and the confinement is illustrated

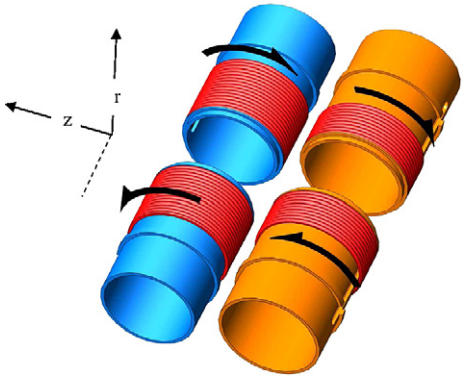

Fig. 2. Schematic of our BiQUIC magnetic trap, consisting of two sets of anti-Helmholtz coils with the current directions as shown.

by the maximum achievable field gradient. Close to the origin the axial and radial B-field of a AH setup is given, to first order, by [21]:

$$B_z \cong \mu_0 3NI \frac{DR^2}{(D^2+R^2)^{5/2}} z, \tag{1}$$

$$B_r \cong -\mu_0 \frac{3}{2} NI \frac{DR^2}{(D^2+R^2)^{5/2}} r, \tag{2}$$

where R is the radius of the coils, $2D$ is the separation, I is the coil current, N is the number of turns on each coil and μ_0 is the permeability of free space. Both the axial and radial field gradients are maximised when the coil geometry is set such that $2D = R$, then,

$$\frac{\mathrm{d}B_z}{\mathrm{d}z} = mu_0 NI \frac{12}{25\sqrt{5}D^2} = 2\frac{\mathrm{d}B_r}{\mathrm{d}r}. \tag{3}$$

Thus the field gradients scale inversely with the square of the separation.

Our trap uses quadrupole coils comprising a single layer of 10 turns and Ioffe coils consisting of a single layer of 18 turns. Both coil sets are approximately ~14 mm in diameter and are wound from 500 μm diameter wire. The centers of the two AH coil sets are displaced in the z direction by 18.5 mm from each other, and with a current of 36 amps the coils generate a trap with a radial gradient of 175 G/cm and an axial curvature of 70 G/cm^2. For helium atoms trapped in the $m = +1$ state this amounts to trapping frequencies of 96 Hz in the radial direction and 650 Hz in the axial direction, for an offset field of 1.9 G.

Water cooling is used to remove heat from the coils, with water running directly over the windings. The use of a single layer allows excellent thermal contact between the water and all the windings, enabling a thermal time constant on the order of seconds. This is an important feature, when one requires shot-to-shot reproducibility. Furthermore, at the maximum current of 36 A the coils only produce 300 W of heat, which is easily removed using a low flow (0.5 l/min) of temperature controlled water (stable to <100 mK), allowing excellent thermal stability. One final advantage of our system is that due to the small coil

separation, our coils are relatively small. Besides the practical advantages of using small coils, they offer improved switching performance. In most experimental BEC systems, the limiting factor in switching off B-fields generated by coils is induced Eddy currents [22]. Eddy currents are generated at switch off by magnetic field lines passing through conductive objects, such as vacuum chambers. By using small coils these field lines fall off quickly, thus reducing the magnitude of generated Eddy currents and improving switch off times.

2.3. Detection

In order to measure the atom number in our experiment we use a saturated fluorescence method [23,24]. The method relies on ramping our MOT laser beams to resonance with full power. In such case, the scattering rate of photons is simply $R = N \times \Gamma/2$, and one need only take into account the collection efficiency of the imaging system to determine the number of atoms. Explicitly, our atom number measurement procedure is as follows. Firstly, we turn off the trap magnetic field, and allow 200 μs for the field to decay away. The measured $1/e$ turn-off time for our magnetic trap coils is 100 μs. The MOT beams are then pulsed on for 50 μs with approximately zero detuning and an intensity many hundred times I_{sat}. We confirm that the sample is saturated by increasing the power of the laser beams until no increase in fluorescence is measured. This process also confirms that the saturation parameter is much larger than the optical thickness of the atom cloud. In this regime there are as many photons exiting the atom cloud as were spontaneously emitted from it [24]. The measured peak fluorescence value can then be used to determine the atom number, which in turn can be used to measure the cloud density once the temperature and trapping frequencies are known. Note that because of our short exposure time the atom cloud does not move significantly during the measurement. A potential source of error is Doppler shifts due to the atoms accelerating during the measurement, we estimate the error due to this process to be 5%. In our measurements we use a high speed InGaAs photodetector capable of rise times less than 50 μs. Our largest error is for small atom numbers of $\sim 1 \times 10^6$, in which case we estimate the error to be ±10%.

To determine the temperature of the trapped atomic sample while operating above the critical temperature, we simply turn-off our magnetic trap and monitor the time-of-flight (TOF) signal produced from an electron multiplier (EM) located directly below the trap. The temperature can then be deduced from fitting the TOF signal to the equation given by [27],

$$n(t) = \int\int A \exp\left(-\frac{\left(\frac{1}{2}gt^2 - l_0\right)^2 + x^2 + y^2}{v_0^2 t^2}\right) \times \frac{\left(\frac{1}{2}gt^2 + l_0\right)^2}{t^4}\,\mathrm{d}x\,\mathrm{d}y, \tag{4}$$

where $A = (m/2\pi k_{\text{b}}T)^{3/2}$, $v_0 = \sqrt{2k_{\text{b}}T/m}$, l_0 is the fall distance, k_{b} is Boltzman's constant, m is the mass of helium, g is the acceleration due to gravity, and the integrals are evaluated numerically over the x and y dimensions of our detector. The fraction of atoms that should strike our detector can also be determined for a particular temperature, by dividing the total integral over our detector by the integration of Eq. (4) over all space. In conjunction with this fraction our saturated fluorescence measurements can then be used to calibrate our TOF signals, so that a total number of atoms can be determined. Comparison of the total number determined this way and by saturated fluorescence alone agree within 30%. In our experiment, when we turn-off our trap the atoms remain in the $m = +1$ state. We have confirmed this by applying B-field gradients during the fall time and observed that in such case the atoms do not strike the EM. The TOF atom number analysis assumes that the cloud is not peturbed during switch off or by magnetic field gradients, which may not be a good assumption for $m = +1$ atoms, and thus is prone to systematic errors.

For clouds below the critical temperature, we use a slightly different experimental procedure. 10 μs before we turn the trap off we pulse on a 10 μs microwave pulse to transfer atoms from the $m = +1$ trapped state to the $m = 0$ untrapped state. The frequency width of this pulse is ~200 kHz and has sufficient power to interact with the entire atomic distribution and transfers approximately one percent of the trapped atoms into the $m = 0$ untrapped state. The atomic cloud is then allowed to freely expand for 50 ms, after which the trapping field is turned back on to stop atoms in the $m = +1$ or $m = -1$ state reaching the EM detector. In this way we probe only magnetic field insensitive atoms which are almost insensitive to imperfections in our trap switch off. The advantage of this procedure over simply turning off the magnetic trap are two-fold. Firstly, we have observed asymmetries in our coldest TOF signals produced by turning off the magnetic trap, which we believe are caused by $m = +1$ atoms interacting with the trap field as it switches. Secondly, any non-uniform magnetic field gradients will distort the trajectories of $m = +1$ atoms and hence yield a distorted TOF signal.

Below the critical temperature we fit the observed TOF signal to a bimodal distribution comprising a thermal part (Bose distribution) and a condensate part (parabolic distribution). From the thermal fit we obtain the temperature of the cloud, and to determine the number of thermal atoms we use the relationship $N_{\text{th}} = 1.202(k_{\text{b}}T/\hbar\widetilde{\omega})^3$ [5], where $\hbar$ is Planck's constant divided by 2π and $\widetilde{\omega}$ is the geometric mean of the trapping frequencies. From the condensate fit we determine the chemical potential which in the Thomas–Fermi limit [25] is given by $\mu^{5/2} = 15\hbar^2 m^{1/2} 2^{-5/2} N_0 \widetilde{\omega}^3 a$, where a is the scattering length, thus yielding the condensate number N_0. Note that for our measurements the relevant scattering length is between $m = +1$ and $m = 0$ atoms. Theoretical models [26] indicate that the

value of this scattering length should be within 5% of the $a = 7.512$ nm measured by Leduc and co-workers [10]. In this way we determine the total number of atoms using only the shape of the TOF signal: we do not require the quantum efficiency of the EM or the fraction of atoms that strike our detector. Comparison of the total number of atoms determined in this way with our saturated fluorescence signal for the same conditions agree to within 25%, as long as the thermal fraction is not less than ~10%. This agreement is reasonable since the comparison is very sensitive to shot-to-shot variations in temperature.

3. Production of a He* Bose–Einstein condensate

Our BEC experimental cycle is as follows: we first load around 5×10^8 atoms into a ultra high vacuum MOT from an LVIS$^+$ atomic beam of He*. To transfer atoms into our magnetic trap we spatially compress the MOT, by tuning the MOT laser frequencies closer to resonance for a period of 2 ms, resulting in a five-fold increase in MOT density. Following compression the MOT magnetic field is switched off and the atoms are further cooled to around 200 μK by applying a 3-D Doppler molasses stage, here we tune both δ_1 and $\delta_2 \sim -2 \times \Gamma$ and reduce the laser intensities for a period of 400 μs.The magnetic trap is then energised with a bias field of 20 Gauss. In such a configuration the trap has very weak trapping frequencies, typically $f_r = 84$ Hz and $f_a = 75$ Hz, which minimises heating of the atomic cloud. At transfer we have around 1×10^8 atoms at a temperature of 1.3 mK. Immediately after transfer we implement a 1-D in trap Doppler cooling scheme, first demonstrated for He* by Vassen and co-workers [11]. A set of weak counterpropagating laser beams ($I \sim 0.01 I_{\text{sat}}$) are aligned at 15 degrees to the bias field of the magnetic trap, polarised such that most atoms cycle back to the low field seeking trapping state. These Doppler cooling laser beams are detuned $\sim -\Gamma/2$ from the Zeeman shifted $m = 1 \rightarrow m = 2$ transition and cool the atoms down to ~200 μK in approximately 350 ms. The bias field of the trap is then adiabatically reduced to 5 Gauss, increasing confinement and subsequently increasing the temperature of the gas. To remove this heat we apply a second Doppler cooling stage which lasts 500 ms, once again achieving a temperature around ~200 μK. TOF traces shown in Fig. 3 illustrate how effective the 1-D Doppler cooling stage is. The upper trace shows a transfer distribution when the 1-D Doppler cooling is not applied, while the lower trace shows the result of using the cooling stage.The bias field is then reduced adiabatically to ~1.9 G at which point, we have 7.5×10^7 atoms at a temperature of ~200 μK, giving an initial phase space density of 5×10^{-5}, an excellent starting point to achieve runaway evaporation. We evaporate in seven seconds using an exponential trajectory comprising seven linear stages. Fig. 4 shows a plot of our phase space density measured throughout our evaporation ramp. We cross the transition temperature at ~2 μK with around two million atoms. TOF distributions are shown in Fig. 5,

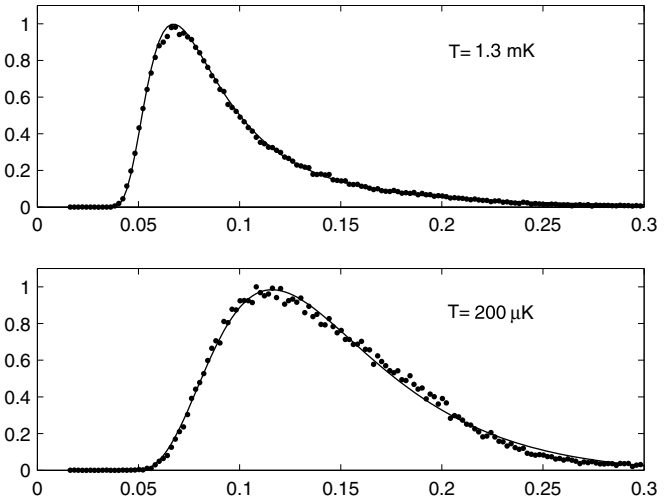

Fig. 3. Time-of-flight distributions taken before (upper trace) and after (lower trace) we implement our 1-D Doppler cooling. The data is shown as (●) and fits to the data are shown as solid lines.

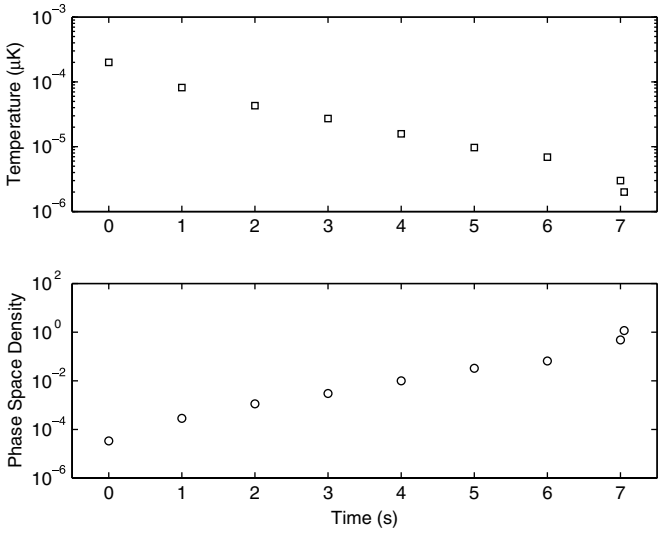

Fig. 4. Plot of temperature and phase space density as a function of evaporation time. At the end of our evaporation ramp we reach the critical temperature with approximately two million atoms at a temperature of 2 μK.

which show different runs of the experiment in which the evaporation frequency has been taken closer to the magnetic trap bottom, thereby producing colder atomic distributions. Each trace is an average of ten runs of the experiment and taken at a bias field of 1.9 Gauss. The upper trace shows a TOF signal taken above the critical temperature, for which a fit of Eq. (4) is also shown and gives a temperature of 2.7 μK. The middle trace shows a TOF signal as the critical temperature is reached, and a fitted curve comprising a thermal part (Bose distribution) and a condensate part (parabolic distribution). As the cloud is cooled further (lower trace), a bimodal distribution is clearly seen indicating the presence of a BEC. In our

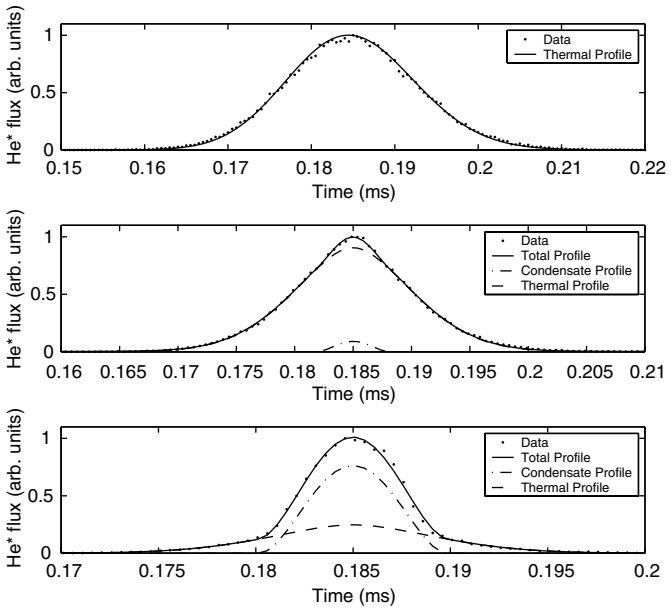

Fig. 5. Time of flight traces taken from an electron multiplier located directly under our magnetic trap. Traces are shown for different final evaporation frequencies, the relevant final frequencies relative to the trap bottom are: upper trace −400 kHz, middle trace −150 kHz, lower trace −100 kHz. Each trace is an average of ten runs of the experiment and taken at a bias field of 1.9 Gauss. The upper trace shows a TOF signal taken above the critical temperature, for which a fit of Eq. (4) is shown and gives a temperature of 2.7 μK. The middle trace shows a TOF signal as the critical temperature is reached, and the fitted curve comprises a thermal part (Bose distribution) and a condensate part (parabolic distribution). The relevant numbers for this trace are, $T = 1.5\ \mu K$, $N_{th} = 8.8 \times 10^5$ and $N_0 = 9.0 \times 10^4$. As the cloud is cooled further (lower trace), a bimodal distribution is clearly seen indicating the presence of a BEC. For this trace $T = 1.0\ \mu K$, $N_{th} = 2.5 \times 10^5$ and $N_0 = 8.4 \times 10^5$.

experiment we typically produce BEC's comprising approximately one million atoms.

The stability of a magnetic trap is important for many types of BEC experiments. Moreover, there are two types of stability that interest the experimentalist, long and short term stability. Long term drifts on the order of tens of seconds cause the trap bottom to vary over successive runs of the experiment, which lead to poor shot-to-shot reproducibility. Short term fluctuations, like AC noise on coil currents, occur within each evaporation cycle and while usually having minimal effect on BEC production they can limit other types of experiments. In our system we control the currents in our coils to around 1 part in 10^5, which amounts to 10 μG of magnetic field noise. However, we have measured our AC trap noise using RF output coupling [28] and determined it to be approximately 5 mG peak-to-peak. The AC trap noise is heavily dominated by 50 Hz oscillations and is consistent with background AC magnetic fields in our laboratory as measured by a calibrated pick-up coil. The long term stability of the trap is very good, providing we allow 3 s of 'cool down' time between each run of the experiment. In such case the shot-to-shot reproducibility of condensate atom number is approximately ±5%.

4. Conclusion

To summarise, we have used a new type of magnetic trap geometry to produce a BEC of metastable helium atoms containing approximately one million atoms. The BiQUIC trap is very stable and at present the noise on our trap is dominated by background AC magnetic fields which are present in our laboratory. The BiQUIC geometry may lend itself to experiments in which large vacuum chambers are used and as such a normal QUIC trap is difficult to implement.

Acknowledgements

The authors wish to acknowledge the technical assistance of Stephen Battisson in the design and construction of the He* beamline and Colin Dedman for producing the magnetic trap switching circuitry. We also acknowledge Lesa Byron for her assistance with the data collection and Ken Baldwin for careful reading of the manuscript. This work is supported by the Australian Research Council Centre of Excellence for Quantum-Atom Optics.

References

[1] M.H. Anderson, J.R. Ensher, M.R. Matthews, C.E. Wieman, E.A. Cornell, Science 269 (1995) 198.
[2] K.B. Davis, M.-O. Mewes, M.R. Andrews, N.J. van Druten, D.S. Durfee, D.M. Kurn, W. Ketterle, Phys. Rev. Lett. 75 (1995) 3969.
[3] C.C. Bradley, C.A. Sackett, J.J. Tollet, R.G. Hulet, Phys. Rev. Lett. 75 (1995) 1687.
[4] F. Pereira Dos Santos, J. Léonard, Junmin Wang, C.J. Barrelet, F. Perales, E. Rasel, C.S. Unnikrishnan, M. Leduc, C. Cohen-Tannoudji, Phys. Rev. Lett. 86 (2001) 3459.
[5] A. Robert, O. Sirjean, A. Browaeys, J. Poupard, S. Nowak, D. Boiron, C.I. Westbrook, A. Aspect, Science 292 (2001) 20.
[6] G.V. Shlyapnikov, J.T.M. Walraven, U.M. Rahmanov, M.W. Reynolds, Phys. Rev. Lett. 73 (1994) 3247.
[7] M. Schellekens, R. Hoppeler, A. Perrin, J. Viana Gomes, D. Boiron, A. Aspect, C.I. Westbrook, Science 310 (2005) 648.
[8] S. Seidelin, O. Sirjean, J. Viana Gomes, D. Boiron, C.I. Westbrook, A. Aspect, J. Opt. B: Quantum Semiclass. Opt. 5 (2003).
[9] J. Léonard, M. Walhout, A.P. Mosk, T. Müller, M. Leduc, C. Cohen-Tannoudji, Phys. Rev. Lett. 91 (2003) 073203.
[10] S. Moal, M. Portier, J. Kim, J. Dugué, U.D. Rapol, M. Leduc, C. Cohen-Tannoudji, Phys. Rev. Lett. 96 (2006) 023203.
[11] A.S. Tychkov, T. Jeltes, J.M. McNamara, P.J.J. Tol, N. Herschbach, W. Hogervorst, W. Vassen, Phys. Rev. A 73 (2006) 031603(R).
[12] Tilman Esslinger, Immanuel Bloch, Theodor W. Hänsch, Phys. Rev. A 58 (1998) R2664.
[13] M.-O. Mewes, M.R. Andrews, N.J. van Druten, D.M. Kurn, D.S. Durfee, W. Ketterle, Phys. Rev. Lett. 77 (1996) 416.
[14] J.A. Swansson, K.G.H. Baldwin, M.D. Hoogerland, A.G. Truscott, S.J. Buckman, Appl. Phys. B 79 (2004) 485.
[15] C.J. Dedman, J. Nes, T.M. Hanna, R.G. Dall, K.G.H. Baldwin, A.G. Truscott, Rev. Sci. Instrum. 75 (2004) 5136.
[16] R.J.W. Stas, J.M. McNamara, W. Hogervorst, W. Vassen, Phys. Rev. A 73 (2006) 032713.
[17] J.A. Swansson, R.G. Dall, A.G. Truscott, Rev. Sci. Instrum. 77 (2006) 046103.
[18] Z.T. Lu, K.L. Corwin, M.J. Renn, M.H. Anderson, E.A. Cornell, C.E. Wieman, Phys. Rev. Lett. 77 (1996) 3331.

[19] J.A. Swansson, R.G. Dall, A.G. Truscott, Appl. Phys. B, accepted for publication.
[20] E.L. Raab, M. Prentiss, A. Cable, S. Chu, D.E. Pritchard, Phys. Rev. Lett. 59 (1987) 2631.
[21] T. Bergeman, G. Erez, H.J. Metcalf, Phys. Rev. A 35 (1987) 1535.
[22] C.J. Dedman, K.G.H. Baldwin, M. Colla, Rev. Sci. Instrum. 72 (2001) 4055.
[23] F. Pereira Dos Santos, F. Perales, J. Léonard, A. Sinatra, Junmin Wang, F. Saverio Pavone, E. Rasel, C.S. Unnikrishnan, M. Leduc, Eur. Phys. J. D 14 (2001) 15.
[24] M.T. DePue, S.L. Winoto, D.J. Han, D.S. Weiss, Opt. Commun. 180 (2000) 73.
[25] F. Dalfovo, S. Giorgini, L.P. Pitaevskii, S. Stringari, Rev. Mod. Phys. 71 (1999) 463.
[26] I.B. Whittingham, personal communications.
[27] I. Yavin, M. Weel, A. Andreyuk, A. Kumarakrishnan, Am. J. Phys. 70 (2001) 149.
[28] M.-O. Mewes, M.R. Andrews, D.M. Kurn, D.S. Durfee, C.G. Townsend, W. Ketterle, Phys. Rev. Lett. 78 (1997) 582.